

estimation. As the burst size is increased, the accuracy of estimation will be improved. The bias is nearly constant at relatively high SNR. The results agree with the results in the time domain [2].

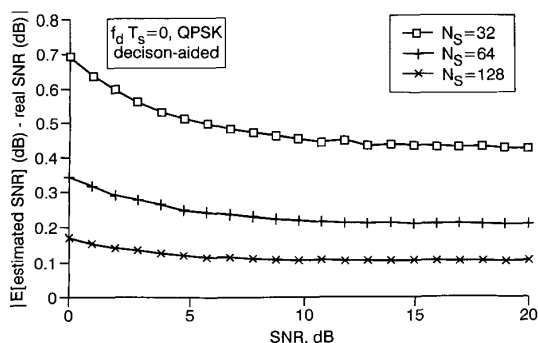


Fig. 1 Bias of the SNR estimation in frequency domain

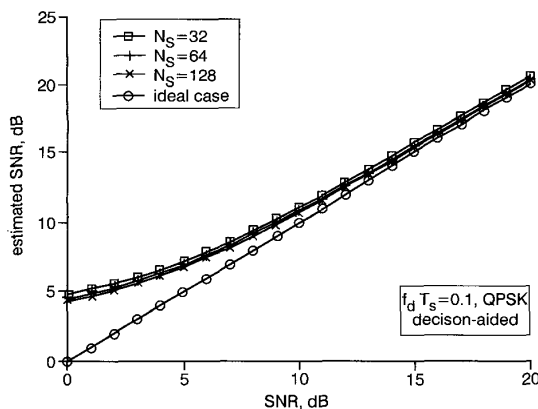


Fig. 2 Performance of SNR estimation using circular correlation

Performance of SNR estimation using circular correlation is shown in Fig. 2, when the normalised frequency offset is 0.1. At low SNR, the accuracy of SNR estimation is not sufficiently precise. This is due to the cross-correlation between the signal and noise. However, at high SNR, the estimation is very accurate irrespective of the burst size. Hence we conclude that the proposed scheme is well suited to digital modems using DFT algorithms.

Conclusions: In this Letter, we proposed SNR estimators for an MPSK modulation in frequency domain. Circular correlation was used for robust SNR estimation when the frequency offset occurs at the received signal. Simulation results showed that the new estimators present good performance even when a large frequency offset occurs.

© IEE 2002

6 June 2002

Electronics Letters Online No: 20021178
DOI: 10.1049/el:20021178

Dae-Ki Hong, Cheol-Hee Park, Min-Chul Ju, Kyu-Jung Youn, Sun-Do Jun and Jin-Woong Cho (Wireless PAN Technology Project Office, Korea Electronics Technology Institute (KETI), Korea)

References

- 1 ALAGHA, N.S.: 'Cramer-Rao bounds of SNR estimates for BPSK and QPSK modulation signals', *IEEE Commun. Letters*, 1998, 5, (1), pp. 10–12
- 2 BEAULIEU, N.C., TOMS, A.S., and PAULUZZI, D.R.: 'Comparison of four SNR estimators for QPSK modulations', *IEEE Commun. Letters*, 2000, 4, (2), pp. 43–45
- 3 PAULUZZI, D.R., and BEAULIEU, N.C.: 'A comparison of SNR estimation techniques for the AWGN channel', *IEEE Trans. Commun.*, 2000, 48, (10), pp. 1681–1691

- 4 MAZZENGA, F., and CORAZZA, G.: 'Blind least-squares estimation of carrier phase, Doppler shift, and Doppler rate for m-PSK burst transmission', *IEEE Commun. Letters*, 1998, 2, pp. 73–75
- 5 MEYR, H., MOENECLAAY, M., and FECHTEL, S.: 'Digital communication receivers' (New York, Wiley, 1998, 1st edn.), Chap. 9

TTCM schemes based on time-varying trellis approach

Sen Jiang, B.M. Bai, Chi Sing Leung, Ping Li and Hong Sun

An efficient time-varying trellis approach is proposed for turbo trellis coded modulation (TTCM). Using a time-varying trellis, the efficient free Euclidean distance is increased, thus improving the performance of TTCM. Experimental results show that the bit error rate (BER) of the proposed time-varying TTCM is better than that of the conventional TTCM scheme. Also, compared with an eight-state time-invariant TTCM scheme, a two-state time-varying TTCM scheme can achieve nearly the same BER performance.

Introduction: Turbo trellis coded modulation (TTCM) is a bandwidth efficient turbo code technique that combines the concepts of iterative decoding and trellis coded modulation (TCM) [1–3]. Many existing TTCM schemes are based on the time-invariant trellis approach [1, 3]. We can improve their BER performance by increasing the number of states used in the trellis. However, it will increase the decoding complexity. In this Letter we introduce a novel time-varying trellis approach for TTCM. With the concept of time-varying trellis, we can improve the BER performance of a TTCM scheme without increasing the number of states used in the trellis.

Time-varying trellis: In a conventional time-invariant trellis code, the trellis pattern, including trellis structure and the distribution of branch labels, does not depend on time instant. In a time-varying trellis code, shown in Fig. 1, the trellis pattern depends on the time instant. This example is a simple two-state time-varying QPSK with a period of 2. The signal constellation $\{s_0, s_1, s_2, s_3\}$ is uniformly selected from a unit circle in anticlockwise order. There are two trellis patterns, namely, *P* and *C*. Pattern *P* has horizontal transitions only, where the state is unchanged regardless of the input symbol. Given an encoding path, if the input in a pattern *P* section is changed, the new encoding path differs from the original path just at this pattern *P* section. Pattern *C* has both cross and horizontal state transitions.

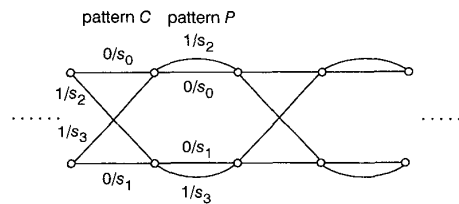


Fig. 1 Time-varying trellis for QPSK

TTCM based on time-varying trellis: We first use a time-varying QPSK TTCM scheme as an illustrative example. The proposed scheme consists of four component trellis codes shown in Fig. 2. Each code is a two-state time-varying QPSK TCM with a period of 4. Patterns *P* and *C* of each component code are similar to those of the code shown in Fig. 1. A random interleaver is used to permute the input bit sequence before each component encoder, which is constrained by

$$\pi(i) \bmod 4 = i \bmod 4 \quad (1)$$

where i and $\pi(i)$ represent the position indices of an information bit before and after interleaving, respectively. All output symbols of pattern *C* sections are punctured. Hence, the code rate is 1 bit/symbol. In the receiver side, there are four soft MAP decoders, connected in a way similar to the conventional TTCM scheme used in [1].

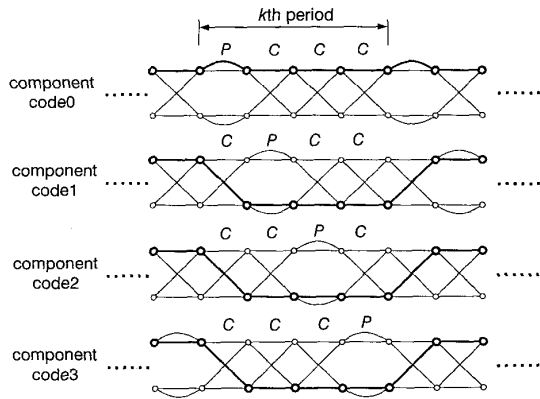


Fig. 2 Four component TCM codes for time-varying TTCM scheme
All output symbols in pattern C sections are punctured

We also construct a time-invariant QPSK TTCM scheme, which consists of four component codes using pattern C only. Hence, the two TTCM schemes have the same decoding complexity. Their performance is depicted in Fig. 3. For block sizes of 1024 and 65 536 bits, the performances of the time-varying TTCM are about 0.2 dB better than those of the time-invariant TTCM at BER = 10^{-5} .

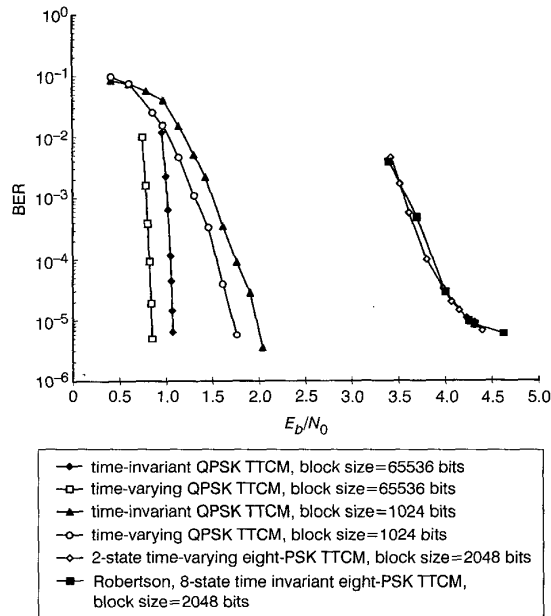


Fig. 3 BER performances for time-invariant and time-varying TTCM schemes with code rates of 1 bit/symbol (QPSK) and 2 bits/symbol (8-PSK)

18 iterations used in all simulations

Effective free Euclidean distance: A heuristic explanation for the good performance of the time-varying trellis QPSK TTCM is as follows. According to [4], the BER performance of a TTCM scheme depends on the effective free Euclidean distance ($D_{free,eff}^f$). It is defined as the minimum Euclidean distance among all pairs of coded sequences, the corresponding input sequences of which have a Hamming distance of 2. It can be verified that the signal mappings in patterns C and P are geometrically uniform [5]. Hence, we can use a coded output sequence (path) Φ , which is generated by an all-zero input bits, as a reference path. This sequence consists of symbols s_0 only. Consider an input sequence \mathbf{u} with a Hamming weight of 2 and the two 1's appear in positions i and j . Let $\pi^{(n)}$ be the interleaver of the n th component code. It permutes the input sequence \mathbf{u} into $\mathbf{u}^{(n)}$. The positions of the two 1's in $\mathbf{u}^{(n)}$ are denoted as $\pi^{(n)}(i)$ and $\pi^{(n)}(j)$, respectively. Without loss of generality, assume $\pi^{(n)}(i) < \pi^{(n)}(j)$.

For the time-invariant TTCM scheme, the encoding sequence in each component code splits from the reference path Φ at the $\pi^{(n)}(i)$ th trellis section and merges with the reference path at the $\pi^{(n)}(j)$ th section. The worst case is $\pi^{(n)}(j) = \pi^{(n)}(i) + 1$ for all $n = 0, 1, 2, 3$. The $D_{free,eff}^f$ of the time-invariant TTCM is given by

$$D_{free,eff}^f = \sqrt{4(\|s_2 - s_0\|^2 + \|s_3 - s_0\|^2)} = \sqrt{24} \quad (2)$$

For the time-varying TTCM scheme shown in Fig. 2, the pattern of the s th section of the n th component codes is given by

$$Pa(s, n) = \begin{cases} \text{pattern } P & \text{for } s \bmod 4 = n \\ \text{pattern } C & \text{for } s \bmod 4 \neq n \end{cases} \quad (3)$$

Define $l \equiv (j \bmod 4)$ and $k \equiv (i \bmod 4)$. Since all interleavers are constrained by (1), we get

$$l = [\pi^{(n)}(j) \bmod 4] \text{ and } k = [\pi^{(n)}(i) \bmod 4] \quad (4)$$

for all n , and $\pi^{(n)}(j) \neq \pi^{(n)}(i) \pmod{4}$

Consider the case, $l \neq k$. If $n = l$, $Pa(\pi^{(l)}(i), l) = \text{pattern } C$ and $Pa(\pi^{(l)}(j), l) = \text{pattern } P$. If $n = k$, we have $Pa(\pi^{(k)}(i), k) = \text{pattern } P$ and $Pa(\pi^{(k)}(j), k) = \text{pattern } C$. According to the characteristics of patterns P and C, the encoding path of the l th (k th) component code will keep diverging from the reference path Φ since it is apart from Φ at the $\pi^{(l)}(i)$ th ($\pi^{(k)}(j)$ th) section. Under the assumption of infinite block size, the Euclidean distance between the coded sequence and the reference ones is also infinite.

Now consider the case $l = k$. If $n = l$, we have $Pa(\pi^{(l)}(j), l) = Pa(\pi^{(l)}(i), l) = \text{pattern } P$, which makes the encoding path of the l th component code differ from the reference path Φ just at the $\pi^{(l)}(j)$ th and $\pi^{(l)}(i)$ th sections. If $n \neq l$, we get $Pa(\pi^{(n)}(j), n) = Pa(\pi^{(n)}(i), n) = \text{pattern } C$. In this case, the encoding path splits from the reference path Φ at the $\pi^{(n)}(i)$ th trellis section and merges with the reference path at the $\pi^{(n)}(j)$ th section. For $l = k$, the difference between $\pi^{(n)}(j)$ th and $\pi^{(n)}(i)$ th is equal to $4q$, where q is a position integer. The worst case is, $\pi^{(n)}(j) = \pi^{(n)}(i) + 4$ for all $n = 0, 1, 2, 3$. The encoding path of each component code for such a worst case is shown by the bold line in Fig. 2. The $D_{free,eff}^f$ of the proposed time-varying TTCM scheme is given by

$$D_{free,eff}^f = \sqrt{2\|s_2 - s_0\|^2 + 3(\|s_2 - s_0\|^2 + 2\|s_1 - s_0\|^2 + 2\|s_3 - s_0\|^2)} = \sqrt{44} \quad (5)$$

The above discussion is based on the assumption of no puncturing effect. Considering the puncturing effect, it can be shown that $D_{free,eff}^f = \sqrt{6}$ and $D_{free,eff}^f = \sqrt{14}$. The above analysis demonstrates the advantage of using the time-varying trellis approach.

High-order signal constellation: The time-varying TTCM scheme with high-order constellation has the following difference from the above QPSK case: (i) replace the bit interleaver by symbol interleaver [1] constrained by an equation similar to (1); (ii) for simple trellises (such as two-state), there are more parallel branches in a trellis section. Despite these differences, the time-varying TTCM scheme with high-order constellation can achieve good performance. We construct an eight-PSK TTCM scheme with four two-state time-varying trellis component codes. The code rate is 2 bits/symbol. There are four trellis patterns in this scheme. The BER performances of our two-state time-varying eight-PSK TTCM scheme and the Robertson eight-state time-invariant eight-PSK TTCM scheme [1] are shown in Fig. 3. It can be observed that both TTCM schemes have similar performance. However, our time-varying 8PSK TTCM scheme has a much lower decoding complexity due to using simple two-state component codes.

Conclusion: We have introduced a time-varying trellis approach for TTCM. Simulation results show that, in QPSK and eight-PSK cases, the time-varying approach is better than the traditional time-invariant approach. Also, the analysis of the effective free Euclidean distance for the time-varying QPSK TTCM is given.

Acknowledgment: This work is supported by a grant from Strategic Research Grant, City University of Hong Kong [Project No. 7001126 (EE)].

Sen Jiang and Hong Sun (College of Electronics and Information, Wuhan University, Wuhan, People's Republic of China)

Chi Sing Leung and Ping Li (Department of Electronic Engineering, City University of Hong Kong, Kowloon, Hong Kong)

E-mail: eeleungc@cityu.edu.hk

B.M. Bai (National Key Laboratory of ISN, Xidian University, Xi'an, People's Republic of China)

References

- ROBERTSON, P., and WORZ, T.: 'Bandwidth-efficient turbo trellis-coded modulation using punctured component codes', *IEEE J. Sel. Areas Commun.*, 1998, **16**, pp. 206–218
- LI, P., and WU, K.Y.: 'Concatenated tree codes: a low complexity, high performance approach', *IEEE Trans. Inf. Theory*, 2001, **47**, pp. 791–799
- BLACKERT, W., and WILSON, S.: 'Turbo trellis coded modulation'. Proc. CISS'96, Princeton, NJ, USA, 1996
- VUCETIC, B., and YUAN, J.: 'Turbo codes: principles and applications' (Kluwer Academic Publishers, 2000)
- BIGLIERLI, E., DIVSALAR, D., MCLANE, P.J., and SIMON, M.K.: 'Introduction to trellis-coded modulation with applications' (MacMillan, New York, 1991)

Complete intensity and chirp characterisation of mW peak power ps pulses at 10 GHz propagating over 308 km in fibre recirculation loop

P.-A. Lacourt, M. Hanna, J.M. Dudley and J.-P. Goedgebuer

Complete intensity and chirp characterisation of 15 ps pulses at a wavelength of 1557 nm propagating over a distance of 308 km in a dispersion-shifted fibre recirculation loop is reported. A novel frequency-resolved optical gating configuration based on wavelength conversion allows pulse characterisation at the 10 mW peak power level.

Introduction: The optimisation of high-capacity telecommunications systems using dispersion management or chirped return-to-zero technologies requires the precise characterisation of the long distance evolution dynamics of picosecond optical pulses [1]. There has thus been extensive interest in developing ultrafast measurement techniques around 1550 nm, and techniques such as second-harmonic generation frequency-resolved optical gating (SHG-FROG) [2], sonogram analysis [3], time-resolved optical gating [4] and pulse spectrogram measurements using an external intensity modulator gate [5] have been demonstrated. A novel variant of FROG using wavelength conversion has been developed recently, with enhanced sensitivity sufficient to characterise the intensity and chirp of unamplified picosecond pulses from gain-switched semiconductor lasers [6]. In this Letter, we use this ultrasensitive FROG geometry to perform intensity and chirp characterisation of mW-peak power picosecond pulse propagation over a distance of more than 300 km in an optical fibre recirculation loop. Although pulse propagation in fibres on long-haul distance scales has previously been studied using indirect measurement techniques [7], direct intensity and chirp measurements using FROG have, to date, been restricted to kW peak power pulses propagating over short sub-km fibre lengths [8, 9]. The results here are the first to report intensity and chirp characterisation at peak power levels and over propagation distances corresponding to realistic telecommunications system parameters.

Experiment: Fig. 1a shows the experimental setup. A gain-switched distributed feedback laser at 1557 nm generates ~15 ps duration (FWHM) pulses at a repetition rate of 10 GHz. The pulses possess a large intrinsic negative chirp due to the gain-switching dynamics.

The pulses are amplified in an erbium-doped fibre amplifier (EDFA) before injection into a recirculating loop via a LiNbO₃ electro-optic (EO) intensity modulator. The recirculation loop consists of a 22 km long span of dispersion-shifted fibre (DSF), an EDFA with noise figure 5 dB, a 1.4 nm bandwidth optical filter, and a synchronised acousto-optic switch (AO1). The loop DSF has zero-dispersion wavelength of 1551 nm and a dispersion slope 0.085 ps/nm² km so the injected pulses propagate in the fibre anomalous dispersion regime. The average power at the DSF input is 1.7 mW. A second synchronised acousto-optic switch at the loop output (AO2) allows the pulses to be coupled into the FROG setup after a specified integral number of loop roundtrips between 1 and 14, corresponding to a maximum propagation distance of 308 km. Characterisation for greater distances was not possible because of depolarisation effects.

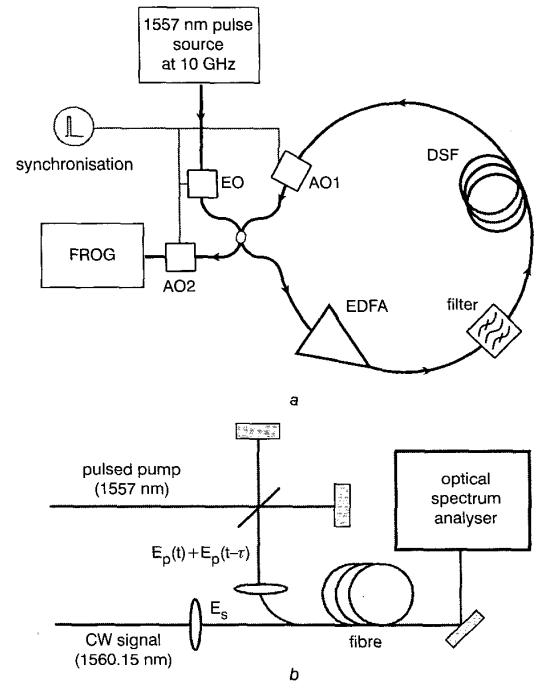


Fig. 1 Experimental setup

a Recirculation loop
b FROG setup

Fig. 1b shows the wavelength conversion FROG setup [6]. Here, the 1557 nm pulse to be characterised is injected into a Michelson interferometer to yield a pulsed pump wave $E_p(t) + E_p(t - \tau)$. This is mixed with a CW signal at 1560.15 nm and launched into a ~20 km length of DSF the ZDW (1557 ± 1) nm of which coincides with that of the pump. Four-wave mixing between the signal and pump generates a wavelength-converted idler the amplitude $E_i \propto E_s * E_p^2$ of which depends quadratically on the pump pulse wave so that the subsequent spectral resolution of the idler against delay yields a FROG trace equivalent to that obtained via SHG. As discussed in more detail in [6], this technique yields accurate intensity and chirp retrieval and mW peak power sensitivity with typical FROG errors <0.5%.

Results and discussion: Fig. 2a shows the intensity retrieved from the FROG measurements plotted every two loop roundtrips at 44 km intervals. The retrieved chirp is also shown at the loop input and after propagation distances of 132 and 308 km. The chirp shows progressive flattening with propagation which has its physical origin in the compensation of the input pulse negative chirp by the positive chirp introduced by nonlinear self-phase modulation (SPM) in the DSF. Previous studies of this phenomenon using kW-peak power femtosecond pulses have shown that this is associated with spectral compression and a decrease in the pulse bandwidth during propagation [8]. This effect was also seen in our experiments, as shown in Fig. 2b. We stress that this nonlinear spectral compression is a result